Electromagnetic Coupling and Radiation Loss Considerations in Microstrip (M)MIC Design

William P. Harokopus, Jr., *Member, IEEE*, and Linda P. B. Katehi, *Senior Member, IEEE*

Abstract—**The high-frequency characterization of microstrip meander lines, junctions, and stubs has been performed by the application of the method of moments to the electric field integral equation. Electromagnetic coupling, radiation, and substrate effects are inherently included with the use of the space-domain Green's function. Conductor loss is also included by replacing the conductive strips with appropriate surface impedance boundaries.**

I. Introduction

FULL-WAVE analysis has been successfully applied to a wide variety of microstrip discontinuities and components [1]–[7]. These techniques are important in high-frequency circuit optimization, because they account for electromagnetic coupling, radiation, and substrate effects. The analysis applied in this paper [6] has previously shown excellent accuracy in the high-frequency characterization of a variety of microstrip structures. Although not a substitute for less intensive approximate techniques (e.g. quasi-static [8]–[12] and dispersive [13]–[16]), this method has proven to be versatile for microstrip characterization in regions where these techniques fail. The aim of this paper is to characterize commonly used microstrip elements in an effort to establish useful design guidelines. In the following sections, results for microstrip meander lines, transmission line junctions, and tuning stubs are presented.

The utilization of the meander line as a phase shifter or slow-wave structure in (M)MIC's is commonplace. Perhaps less well known is the usefulness of meander lines as narrow-band filters. Examples will be given that demonstrate the effect of electromagnetic coupling on the properties of the line and that quantify return, radiation, and conductor losses for a phase shifting section. Also, a meander line having a pencil-thin passband will be shown.

Transmission line junctions are the most commonly used microstrip structures in (M)MIC's. Often, their nonideal effects may be neglected. Nevertheless, radiation loss can become significant in bend and T-junction discontinuities at high frequencies. Furthermore, tapering or mitering of junctions is often done to reduce return loss, but the corresponding effect on radiation is not known. Results on radiation loss will be presented for right-angle and mitered bends, and multiport tee and cross junctions.

The last class of structures presented in this paper comprise tuning stubs, which are frequently used in matching networks of (M)MIC amplifiers and oscillators. In the design of input-matching stages for amplifiers, there exists a keen interest in the reduction of radiation loss, which in turn will improve noise performance. Several stub geometries will be presented, and an evaluation will be conducted of their bandwidths and radiation losses. Furthermore, a matching circuit for a 94 GHz oscillator will be examined to illustrate the effect that electromagnetic coupling and radiation loss have on performance.

Manuscript received April 19, 1990; revised October 22, 1990. This work was supported by the U.S. Army Research Office under contract DAAL03-k-0088(23836-EL) and by the Hughes Malibu Research Laboratories.

The authors are with the Electrical Engineering and Computer Science Department, University of Michigan, Ann Arbor, MI 48109.

IEEE Log Number 9042348.

II. Theory

The microstrip structure is shown in Fig. 1(a). The conductors are lossless and their thickness (t) is much smaller than a wavelength. The substrate is of thickness h and is also assumed lossless. The electric field may be written in terms of an integral equation,

$$\boldsymbol{E}(x,y,z) = \int\int_{S'} \left[k_i^2 \bar{\bar{I}} + \bar{\nabla}\bar{\nabla}\right] \cdot \bar{\bar{G}}(x,y,z/x',y',z') \cdot \boldsymbol{J}(x',y')\, ds', \qquad i = 0,1 \quad (1)$$

with k_0 and k_1 being the wavenumbers in the free-space and dielectric regions, respectively, and where

$$\boldsymbol{J}(x',y') = J_x(x',y')\hat{x} + J_y(x',y')\hat{y} \quad (2)$$

is the current on the microstrip conducting strips. The components of the dyadic Green's function

$$\bar{\bar{G}}(x,y,z/x',y',z') = G_{xx}\hat{x}\hat{x} + G_{zx}\hat{z}\hat{x} + G_{yy}\hat{y}\hat{y} + G_{zy}\hat{z}\hat{y} \quad (3)$$

0018-9480/91/0300-0413$01.00 ©1991 IEEE

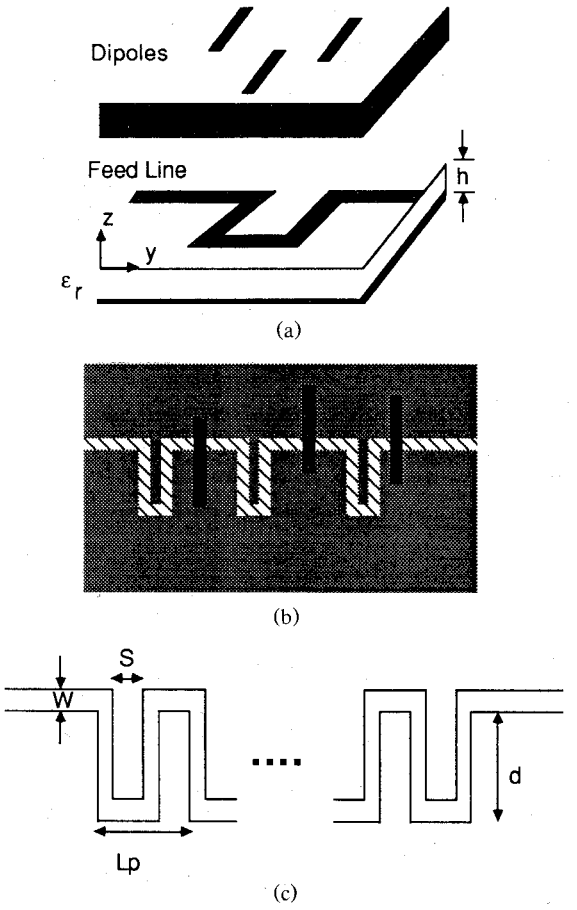

Fig. 1. Geometry of microstrip meander line feeding dipoles. (a) Cross-sectional view. (b) Top view. (c) Meander line parameters.

are expressed in the form of Sommerfeld integrals:

$$G_{xx} = G_{yy} = -\frac{j\omega\mu_0}{2\pi k_0^2}\int_0^\infty J_0(\lambda\rho)u_0\frac{e^{-u_0 z}\sinh uh}{f_1(\lambda,\epsilon_{r1},h)}\lambda\, d\lambda, \quad Z>0 \tag{4}$$

$$G_{zx} = \cot(\phi)G_{zy} = -\frac{j\omega\mu_0}{2\pi k_0^2}(1-\epsilon_r) \cdot \cos\phi\int_0^\infty J_1(\lambda\rho)\frac{e^{-u_0 z}\sinh uh\cosh uh}{f_1(\lambda,\epsilon_{r1},h)f_2(\lambda,\epsilon_{r1},h)}\lambda^2 d\lambda \tag{5}$$

$$G_{xx} = G_{yy} = -\frac{j\omega\mu_0}{2\pi k^2}\int_0^\infty J_0(\lambda\rho)\frac{\sinh u(z+h)}{f_1(\lambda,\epsilon_{r1},h)}\lambda\, d\lambda, \quad Z<0 \tag{6}$$

$$G_{zx} = \cot(\phi)G_{zy} = -\frac{j\omega\mu_0}{2\pi k^2}(1-\epsilon_r) \cdot \cos\phi\int_0^\infty J_1(\lambda\rho)\frac{\sinh uh\cosh u(z+h)}{f_1(\lambda,\epsilon_{r1},h)f_2(\lambda,\epsilon_{r1},h)}\lambda^2 d\lambda \tag{7}$$

with $\rho=\sqrt{(x-x')^2+(y-y')^2}$, $u_0=\sqrt{\lambda^2-k_0^2}$, and $u=\sqrt{\lambda^2-k_1^2}$. The zeros of the functions $f_1(\lambda,\epsilon_{r1},h)$ and $f_2(\lambda,\epsilon_{r1},h)$, given by

$$f_1(\lambda,\epsilon_{r1},h) = u_0\sinh uh + u\cosh uh \tag{8}$$

$$f_2(\lambda,\epsilon_{r1},h) = \epsilon_r u_0\cosh uh + u\sinh uh \tag{9}$$

represent the excited surface wave modes. In (8) and (9), ϵ_r is the relative dielectric constant, and h is the thickness of the substrate.

Resistive losses may also be included by replacing the conductive strips with the appropriate surface impedance boundaries [18], [19]. The boundary conditions on the strip conductors are imposed through the following relation:

$$\boldsymbol{E}_t(x,y,z=t) = \overline{\overline{Z}}\cdot(\boldsymbol{H}\times\hat{z}), \qquad x,y\in S \tag{10}$$

where $\boldsymbol{E}_t$ is the tangential electric field over the surface (S) of the conducting strips and

$$\overline{\overline{Z}}(f) = z_x\hat{x}\hat{x} + z_y\hat{y}\hat{y} \tag{11}$$

represents the appropriate surface impedance boundaries. The magnetic field is related to current on the strip conductor by the expression

$$\hat{z}\times\boldsymbol{H} = \boldsymbol{J}(x',y'). \tag{12}$$

In view of (12), (1) takes the form

$$\int\int_{S'}\left[k_0^2\bar{\bar{I}} + \overline{\nabla}\overline{\nabla}\right]\cdot\overline{\overline{G}}(x,y,z/x',y',z') \cdot\boldsymbol{J}(x',y')\,ds' + \overline{\overline{Z}}\cdot\boldsymbol{J}(x',y') = 0. \tag{13}$$

These frequency-dependent impedance boundaries are evaluated by a quasi-TEM analysis in such a way that they provide the overall effect of the penetration of the fields and the resulting current distributions within the strips [21]. This technique has provided very accurate results for conductor loss at millimeter-wave frequencies [22].

For open microstrip structures at microwave frequencies, radiation losses from discontinuities dominate conductor losses unless long line lengths are present. In this work, the formulation will account for conductor loss in a long meander delay line example. In all other examples perfect conductors will be considered ($\boldsymbol{E}_t(x,y,z=t)=0$).

The microstrip discontinuity is subdivided into squares, and the method of moments is applied with rooftop basis functions. The unknown current is expressed in the form of double summations shown below:

$$J_x = \sum_{n=1}^{N+1}\sum_{m=1}^{M+1} I_{nm}^x j_{nm}^x(x',y') \tag{14}$$

$$J_y = \sum_{n=1}^{N+1}\sum_{m=1}^{M+1} I_{nm}^y j_{nm}^y(x',y') \tag{15}$$

where

$$j_{nm}^x(x',y') = [f_n(x')g_m(y')] \tag{16}$$

$$j_{nm}^y(x',y') = [g_n(x')f_m(y')]. \tag{17}$$

In (14) and (15), I_{nm} is the unknown current amplitude at the (n,m)th position of the subdivided element. The functions f_n and g_m are subdomain shaping or basis functions and are consistent with the current boundary conditions. The

rooftop subdomain basis functions have piecewise-sinusoidal variation in the longitudinal direction and constant variation in the transverse direction according to

$$f_n(x') = \begin{cases} \dfrac{\sin k_s(x_{n+1} - x')}{\sin k_s l_x}, & x_n \leq x' \leq x_{n+1} \\ \dfrac{\sin k_s(x' - x_{n-1})}{\sin k_s l_x}, & x_{n-1} \leq x' \leq x_n \\ 0, & \text{else} \end{cases} \tag{18}$$

and

$$g_m(y') = \begin{cases} 1, & y_m \leq y' \leq y_{m+1} \\ 0, & \text{else.} \end{cases} \tag{19}$$

In the above, $l_x = x_{n+1} - x_n$, and k_s is a scaling parameter chosen to vary between k_0 (free-space wavenumber) and k_1 (wavenumber in the dielectric).

Substitution of the above into the electric field integral equation, (1), and application of Galerkin's method result in the matrix equation

$$[Z][I] = [V]$$

where Z is the impedance matrix, and I is the vector of unknown x and y current amplitudes. The vector V is the excitation vector, which is identically zero everywhere except at points where sources are located. In order to excite the discontinuity, voltage gap generators are utilized. The presence of the infinitesimally small gap is reflected in the excitation vector where

$$V_x^{\nu\mu} = \begin{cases} 1 & \text{if } x_\nu = x_g \\ 0 & \text{else} \end{cases} \tag{20}$$

and

$$V_y^{\nu\mu} = \begin{cases} 1 & \text{if } y_\mu = y_g \\ 0 & \text{else.} \end{cases} \tag{21}$$

When a single microstrip mode is excited along the feeding line, the current forms TEM-like standing waves. Under this assumption, the microstrip element may be represented as an N-port network with the port voltages and currents related according to

$$V_n = \sum_{m=1}^{N} Z_{nm} I_m \qquad \forall n \in (1, N). \tag{22}$$

Dividing each voltage V_n by the corresponding current I_n results in the following expression for the input impedance Z_{in_n} at port n:

$$Z_{\text{in}_n} = \sum_{m=1}^{N} Z_{nm} \left(\frac{I_m}{I_n} \right). \tag{23}$$

The input impedances Z_{in_n} and reflection coefficients Γ_n, $(n = 1, N)$, are determined for each port at a given reference plane from the microstrip current solution. An N-port discontinuity has N^2 unknown network parameters. This number can be reduced with reciprocity and symmetry, as done in previously [6], but in general N^2 independent equations are required. These may be obtained from (23) after exciting the N-port microstrip element by N independent excitations.

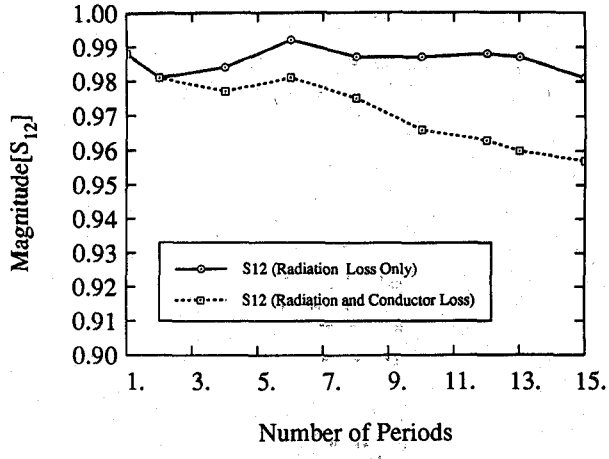

Fig. 2. Transmission parameter magnitude of meander line as a function of length ($f = 20$ GHz, $\epsilon_r = 2.2$, $h = 20$ mil, $W = 10$ mil, $S = 40$ mil, $d = 50$ mil, $t = 12$ μm, $\sigma = 4 \times 10^7$ S/m).

III. Meander Lines

Meander lines are often used in (M)MIC's as delay or slow-wave lines and in monolithic antenna arrays for the phasing of the radiating elements as shown in Fig. 1. In this application, a two-layer structure is shown with an embedded meander line feeding the antenna elements on the top of the substrate. Such a feed structure is also capable of exciting a slot array. The ability to adjust the spacing (S), the depth (d), the period length (L_p), and the number of periods (N) provides flexibility in the phasing of the radiating elements. Therefore, meander lines are particularly suited for use in beam forming and steering [25]. Successful design of such structures requires accurate models, which include the presence of bend discontinuities and the effect of electomagnetic coupling. Radiation and conductor losses may also have significant effects.

Fig. 2 presents the transmission parameter as a function of line length for a meander line on a 20 mil Duroid substrate ($\epsilon_r = 2.2$) at 20 GHz. Two cases are shown: 1) with both resistive and radiation loss and 2) with radiation loss only. In this example, the substrate is electrically thin and radiation loss is not large. Conductor loss is essentially the difference between the two curves, and increases steadily with line length. This example illustrates an interesting point concerning the relative importance of radiation and resistive losses. Radiation losses in microstrip circuits are associated with fringing fields present at discontinuities, and are minimized through the reduction of the number of discontinuities, through the use of electrically thin substrates, and through creative designs—to be discussed further in the following sections. Resistive loss depends on the composition and shape of conductors, and increases with line length. For the following examples, where discontinuities are considered with relatively short lengths of line, only radiation loss will be included.

The unit phase delay (Pd_1) can be defined as the phase shift (Pd) of the line divided by the number of periods (N). To demonstrate the effect that the cascading of several sections has on the phase, a meander delay line on a 25 mil alumina substrate has been analyzed. In Fig. 3, the unit phase delay is shown as a function of frequency for cascades of one, two, and three periods, respectively. The simulation

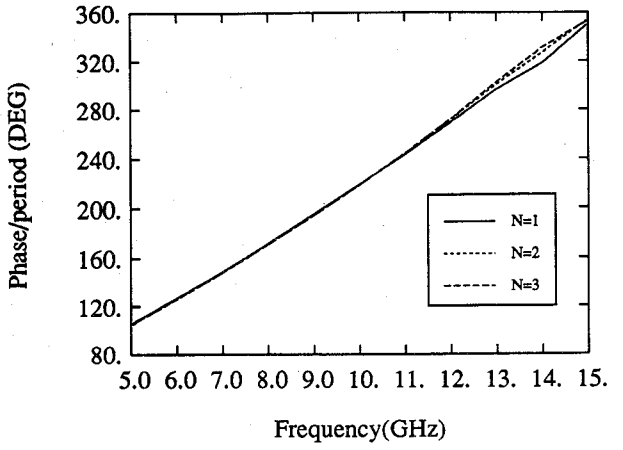

Fig. 3. Phase of transmission parameter for meander line as a function of frequency ($\epsilon_r = 9.978$, $h = 25$ mil, $W = 0.305$ mm, $S = 4W$, $d = 5W$).

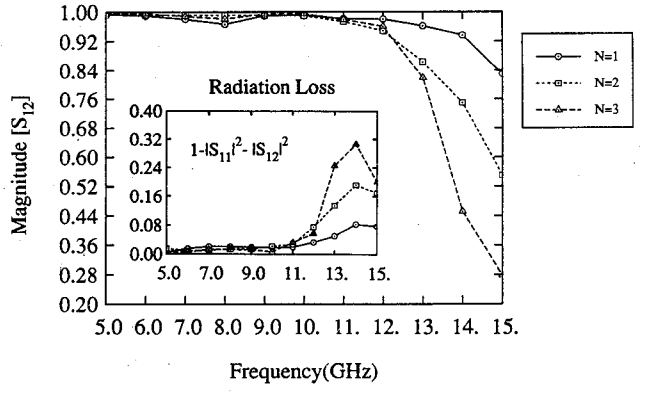

Fig. 4. Magnitude of transmission parameter for meander line as a function of frequency ($\epsilon_r = 9.978$, $h = 25$ mil, $W = 0.305$ mm, $S = 4W$, $d = 5W$).

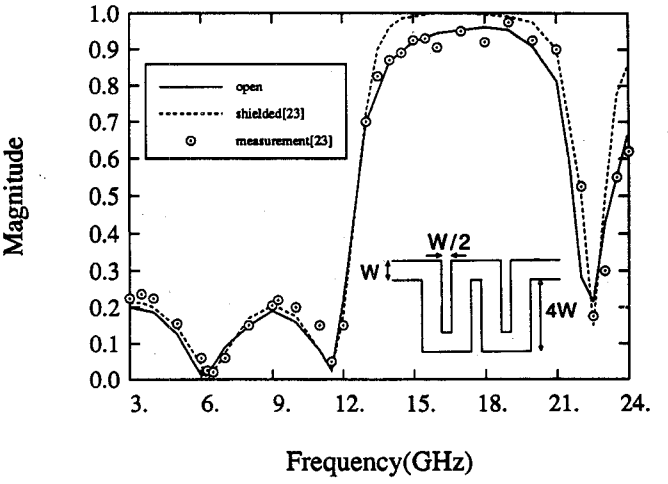

Fig. 5. Magnitude of reflection coefficient for meander line filter as a function of frequency ($\epsilon_r = 9.978$, $h = 25$ mil, $W = 0.61$ mm, $S = 1/2W$, $d = 4W$).

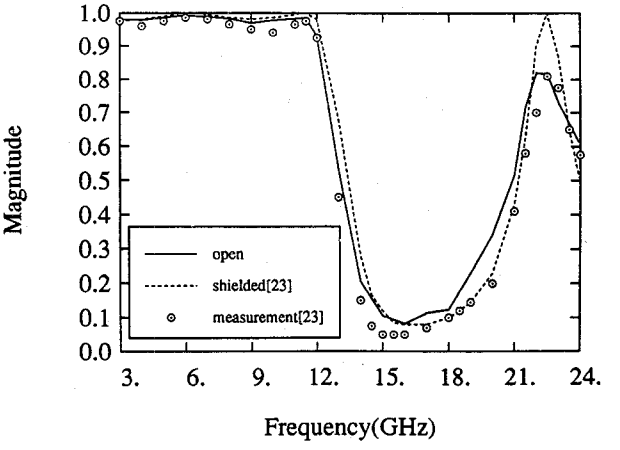

Fig. 6. Magnitude of transmission parameter for meander line filter as a function of frequency ($\epsilon_r = 9.978$, $h = 25$ mil, $W = 0.61$ mm, $S = 1/2W$, $d = 4W$).

for the cascade of three periods was performed with 120 basis functions (including both current components), and it required 392 s (elapsed time) per frequency point on a DEC 3100 workstation. As shown, the unit phase delay is independent of the length of the line from 5 to 12 GHz. Thus, it can be used to accurately determine the phase for a line having many cascaded sections ($pd_N = N \times pd_1$). Deviations in the linear phase characteristic at the high-frequency end result from high radiation and return losses. Shown in Fig. 4 is the transmission parameter of the line for the same cases. Also given in the inset are the radiation losses. In this example, the line has good transmission below 13 GHz, but the performance deteriorates rapidly after that. Furthermore, at high frequencies, the transmission through the line decreases while the radiation loss increases with line length. From these observations, in addition to acting as a delay line, the meander line is particularly well suited for filtering applications. This is true because the spacing and number of periods control the passband corner frequencies and slopes, respectively. This is a well-known characteristic of periodic structures in general [26]–[29].

Shown in Figs. 5 and 6, our theoretical results are compared with theoretical results and experimental data derived by Jansen [23], [24] for shielded and open meander lines, respectively. The simulation was done with 364 basis functions and required 671 s of elapsed time per frequency point on a DEc 3100 workstation. There is good agreement between the open experimental results and our simulation. This structure has two passbands over the frequency range shown. Radiation losses are quite severe and result in degradation of the transmitted power in the 13–20 GHz stopband and the pencil-thin passband centered at 22.5 GHz. In particular, notice the difference at 22.5 GHz between the open and shielded simulations. This example illustrates that meander lines may be useful for narrow-band applications in monolithic arrays, although radiation losses can be severe.

IV. Junctions

Transmission line junctions are found in virtually every type of microstrip layout and are integral parts of power splitters, matching networks, and couplers. Consequently, a thorough understanding of their parasitic behavior is crucial in high-frequency (M)MIC design.

Fig. 7 displays the network parameters for mitered and right-angle-bend discontinuities. The mitered case has supe-

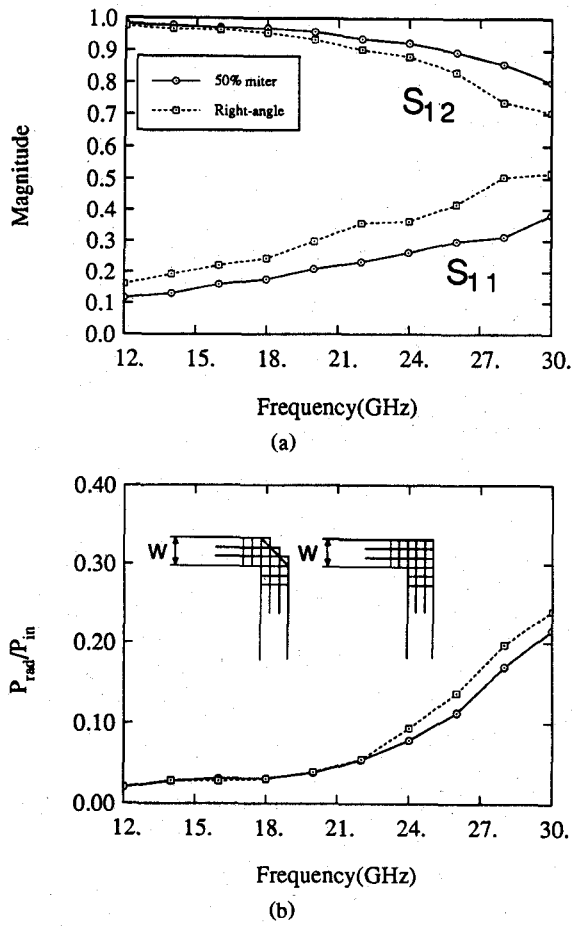

Fig. 7. Scattering parameters (magnitude) for right-angle and mitered bends ($\epsilon_r = 12$, $h = 25$ mil, $W = 15$ mil). (a) Scattering parameters. (b) Radiation loss.

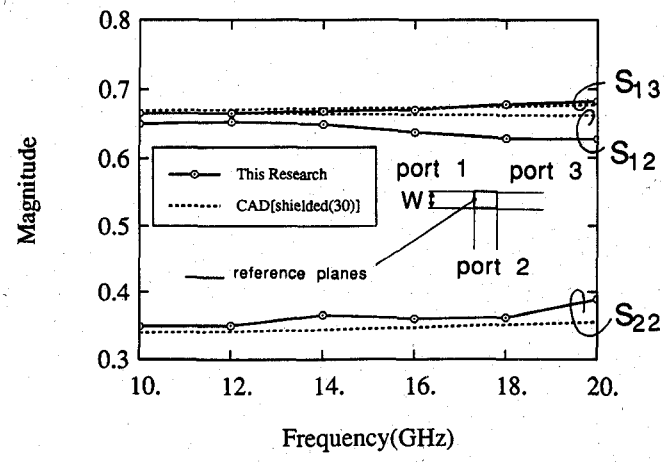

Fig. 8. Scattering parameters (magnitude) for microstrip T junction as a function of frequency ($\epsilon_r = 2.2$, $h = 25$ mil, $W = 25$ mil).

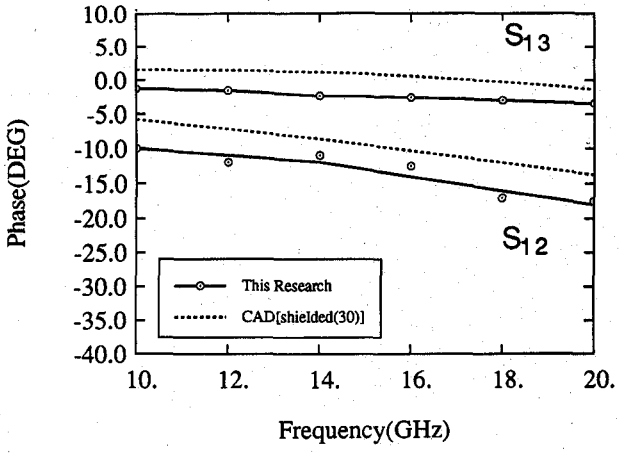

Fig. 9. Scattering parameters (phase) for microstrip T junction as a function of frequency ($\epsilon_r = 2.2$, $h = 25$ mil, $W = 25$ mil).

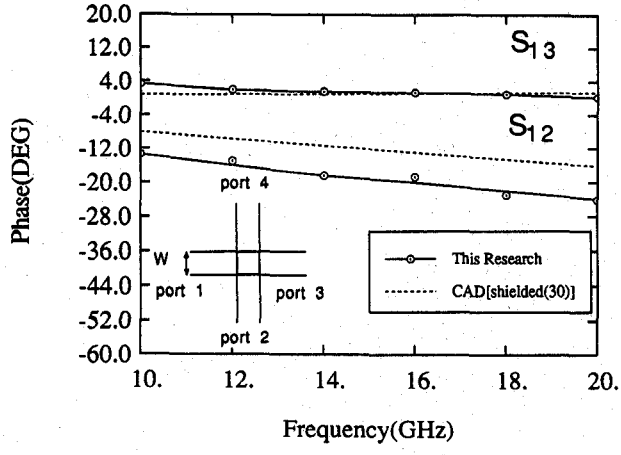

Fig. 10. Scattering parameters (phase) for microstrip cross junction as a function of frequency ($\epsilon_r = 2.2$, $h = 25$ mil, $W = 25$ mil).

rior behavior, as illustrated by its improved return loss. The two structures exhibit almost identical radiation properties (as shown in Fig. 7(b)) below 22 GHz; however, the mitering results in lower radiation loss above 22 GHz. It is concluded that the mitering sharply lowers the return loss by decreasing the excess capacitance of the bend, and also decreases radiation losses at higher frequencies. For further improvement in performance, a multiple-layer substrate may be utilized to lower radiation loss [6].

Following the method described previously, network parameters have been extracted for three-port T-junction and four-port cross junction discontinuities, with interesting results. As shown in Fig. 8, the magnitude of the S parameters of a T junction on a 25 mil Duroid ($\epsilon_r = 2.2$) substrate agree well with available CAD results [30]. On the other hand, as shown in Figs. 9 and 10 for cross and T junctions respectively, the phase can disagree appreciably with those predicted by commercial CAD, particularly between ports at right angles. The disagreement arises from the parasitic reactance and radiation loss (Fig. 11) at the junction.

Also shown in Fig. 11 are the radiation losses of a right-angle bend having the same strip width and printed on the same substrate. The three types (right-angle-bend, cross, and T) of junctions exhibit similar radiation losses. The lowest loss corresponds to the cross junction, which is the only one of the three not having a port current terminate at an edge.

V. Stubs

Open circuit stubs are often used in microstrip matching networks, particularly in (M)MIC amplifiers. Radiation loss and spurious coupling from a matching network have a direct impact on the noise performance of an amplifier and must

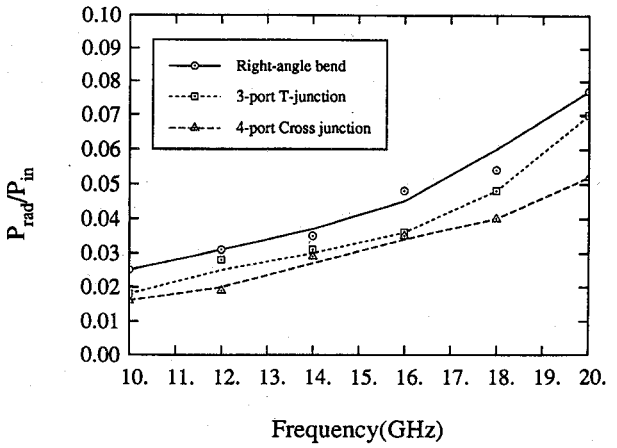

Fig. 11. Radiation Loss for microstrip junctions ($\epsilon_r = 2.2$, $h = 25$ mil, $W = 25$ mil).

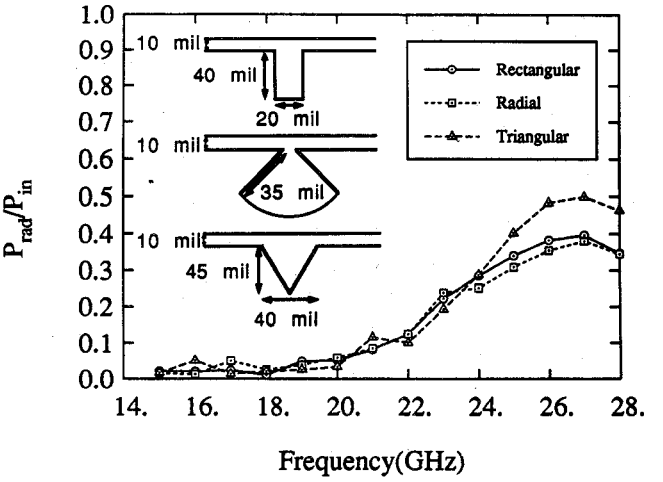

Fig. 13. Radiation loss of microstrip stubs ($\epsilon_r = 12$, $h = 25$ mil).

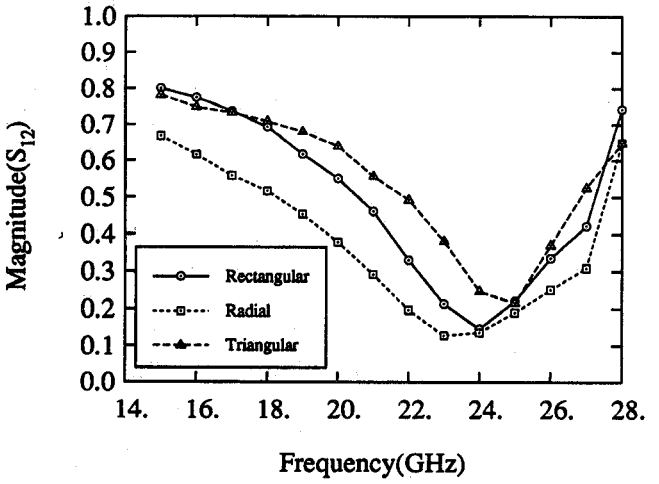

Fig. 12. Transmission parameter of microstrip stubs ($\epsilon_r = 12$, $h = 25$ mil).

therefore be minimized. Several stub geometries have been proposed for enhancing various circuit characteristics including reduced loss. The full-wave analysis presented has been employed to evaluate three types of stubs: a) rectangular, b) radial, and c) triangular in terms of their bandwidth, resonance characteristics, and radiation properties. The stubs are printed on a 25 mil GaAs substrate ($\epsilon_r = 12$) and have the dimensions shown in Fig. 13. For comparison purposes, all of the stubs are designed to have first resonance at about 24 GHz. Two-port scattering parameters have been obtained by positioning the stubs in shunt fashion across a transmission line, as shown. At resonance, the magnitude of the transmission parameter reaches a minimum. Fig. 12 shows the transmission parameters for the three cases from 15 to 28 GHz. As shown, the radial stub has the broadest bandwidth, and the triangular stub has the narrowest. These results indicate that the bandwidth may be adjusted by varying the angle of the radial stub. However, it should be noted that such a modification will also shift the resonant frequency.

As previously mentioned, radiation from matching networks has a direct and derogatory effect on noise performance in (M)MIC amplifiers. Fig. 13 shows quite clearly that the triangular shape radiates more than the other two types, which have similar radiation properties (the radial stub showing moderate improvement over the rectangular type). The loss peaks for all three cases at 27 GHz (about 3–4 GHz beyond resonance), indicating that the radiation properties are heavily influenced by the characteristics of the substrate. For the given substrate at this operating frequency, the loss is primarily due to the TM_0 substrate mode. We conclude that since the triangular stub has the smallest bandwidth, and radiates most severely, it is recommended only for narrow-band applications, where higher losses can be tolerated. The rectangular and radial stubs have similar radiation properties, with the radial stub having a broader band response.

Matching Circuit for 94 GHz Oscillator

Fig. 15(a) shows a matching circuit for a submillimeter-wave oscillator designed to operate at 94 GHz. The network is printed on 100 μm GaAs ($\epsilon_r = 12.8$). The analysis was applied to obtain scattering parameters individually for the cross junction stub (stub A), the T-junction stub (stub B), and the entire matching section. The results presented in this section are normalized to 50 Ω. Of interest in this analysis are the radiation losses experienced as the stubs pass through a quarter-wave resonance, and the coupling between the stubs. Frequently, such a design would be done with available CAD by individually modeling the two stubs, and then chaining together the S parameters. Therefore, electromagnetic interactions between the stubs would not be included.

Shown in parts (a) and (b) of Fig. 14 are the scattering parameters for the cross junction and the T-junction stub, respectively. The quarter-wave resonances of the stubs are 145 GHz for stub A and 160 GHz for stub B, as determined by the minima in the magnitude of S_{12}. There is appreciable radiation loss beyond the resonances of the two stubs. This radiation causes a degradation in the magnitude of S_{11} at the high-frequency end of the simulations for both stubs. The T-junction stub radiates more power than the cross junction stub. In fact, as shown in Fig. 16, at 200 GHz it is radiating almost half of its input power. The lower radiation from the cross junction stub is due to phase cancellation in the radi-

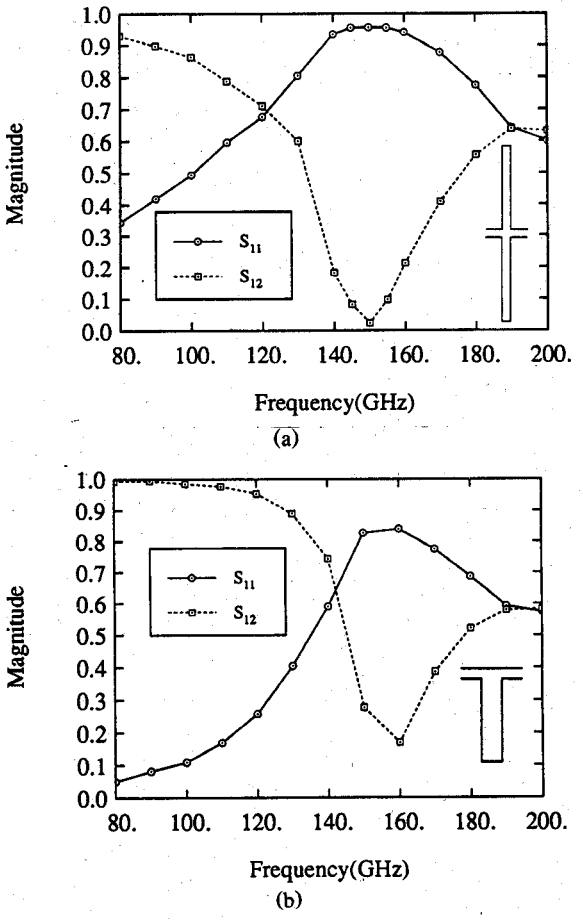

Fig. 14. Scattering parameters of individual stubs found in oscillator matching circuit ($\epsilon_r = 12.8$, $h = 100$ μm, $W = 15.38$ μm). (a) Scattering parameters of stub A. (b) Scattering parameters of stub B.

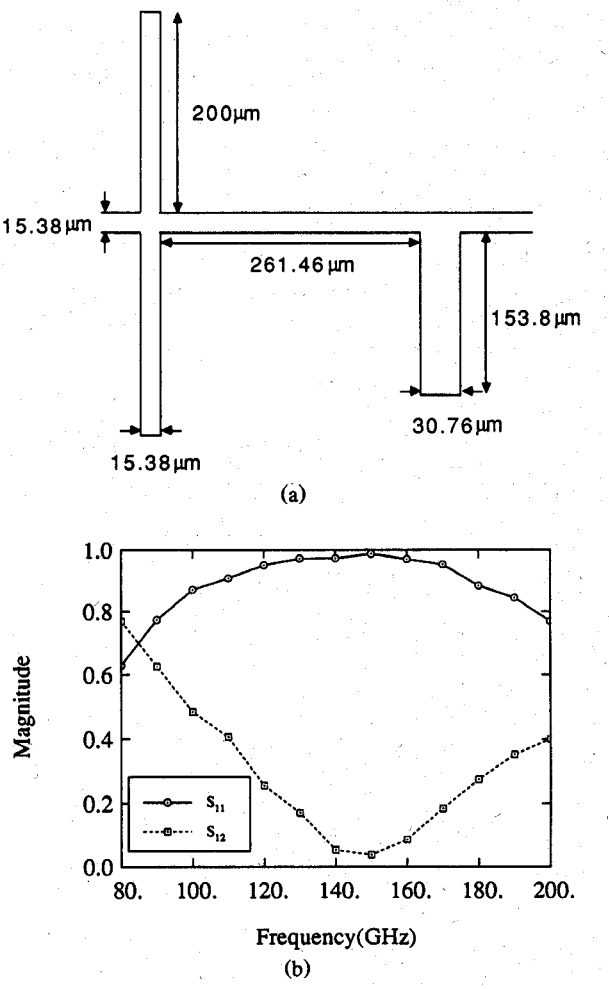

Fig. 15. Scattering parameters of microstrip matching network ($\epsilon_r = 12.8$, $h = 100$ μm, $W = 15.38$ μm). (a) Oscillator matching network. (b) Scattering parameters.

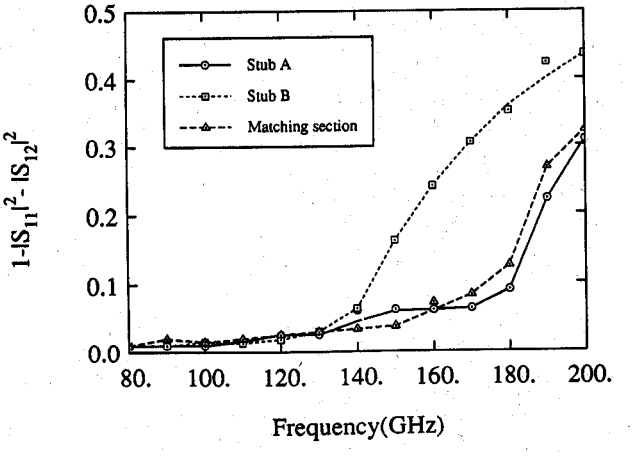

Fig. 16. Radiation loss in microstrip matching network ($\epsilon_r = 12.8$, $h = 100$ μm, $W = 15.38$ μm).

ated fields from the equal and oppositely directed currents on its two arms.

The scattering parameters for the entire matching network are shown in Fig. 15(b). At the lower frequency ranges (below 140 GHz), the radiation losses are not significant. Thus, the network should function adequately at the oscillation frequency. In this example, although the 100 μm substrate is physically thin for present technology, it becomes electrically thick at higher frequencies (one fifth of a wavelength in the dielectric at 170 GHz), and high radiation losses are encountered, as shown in Fig. 16. This result illustrates the difficulty with using microstrip circuits at submillimeter-wave frequencies.

The entire matching network radiates less than stub B alone. At first glance this appears anomalous, but it is a result of the higher return loss of the entire matching network and additional phase cancellation between the stubs. The spacing of the stubs is approximately one half wavelength at the upper frequencies.

VI. Conclusion

The high-frequency behavior of a wide range of open microstrip elements has been presented. Results were obtained by the space-domain integral equation approach which includes all electromagnetic coupling and radiation effects. In addition, resistive loss was included through the replacement of the microstrip conducting strips by surface impedance boundaries. This results in an analysis of irregular microstrip discontinuities which accounts for both resistive and radiation losses. The previous sections included examples of microstrip meander lines, bends, multiport junctions, and tuning stubs.

Two applications of meander lines were shown. First, the effects of radiation and conductor losses on meander line phase shifting sections were presented. These loss mechanisms were shown to reduce the transmission through the line at higher frequencies and longer lengths. Also, an example was given which demonstrated that a long meander line can be accurately characterized by just one of its periods. The second application demonstrates the meander line's filter properties, with an example exhibiting a very narrow passband.

Scattering parameters and radiation losses for several microstrip junctions were presented. The favorable effect of mitering on the return and radiation losses for a bend discontinuity was demonstrated. Furthermore, it was shown that bend, cross, and T junctions printed on a common substrate with the same line width exhibited similar radiation properties.

In the final section, three stub geometries, rectangular, radial, and triangular, were investigated. The radial stub was shown to have the broadest bandwidth of the three, with radiation properties comparable to those of the rectangular stub. The triangular stub had the narrowest bandwidth and the severest radiation loss.

The final example is a matching circuit for a submillimeter-wave oscillator. This example demonstrated that a stub in a cross configuration (two tuning stubs and a cross junction) may have lower radiation loss than a single T-junction stub. Also, the example demonstrates that radiation loss and electromagnetic interactions between stubs in close proximity can have a significant influence on circuit performance.

Acknowledgment

The authors express their gratitude to Dr. A. C. Cangellaris at the University of Arizona for his contributions to this work.

References

[1] P. B. Katehi and N. G. Alexopoulos, "Frequency-dependent characteristics of microstrip discontinuities in millimeter-wave integrated circuits," *IEEE Trans. Microwave Theory Tech.*, vol. MTT-33, pp. 1029–1035, Oct. 1985.

[2] R. W. Jackson and D. M. Pozar, "Full-wave analysis of microstrip open-end and gap discontinuities," *IEEE Trans. Microwave Theory Tech.*, vol. MTT-33, pp. 1036–1042, Oct. 1985.

[3] N. G. Alexopoulos, P. B. Katehi, and D. Rutledge, "Substrate optimization for integrated circuit applications," *IEEE Trans. Microwave Theory Tech.*, vol. MTT-31, pp. 550–557, July 1983.

[4] R. Jackson, "Full-wave finite element analysis of irregular microstrip discontinuities," *IEEE Trans. Microwave Theory Tech.*, vol. 37, pp. 81–89, Jan. 1989.

[5] J. R. Mosig, "Arbitrarily shaped microstrip structures and their analysis with a mixed potential integral equation," *IEEE Trans. Microwave Theory Tech.*, vol. 36, pp. 314–323, Feb. 1988.

[6] W. P. Harokopus, Jr., and P. B. Katehi, "An accurate characterization of open microstrip discontinuities including radiation losses," *IEEE Trans. Microwave Theory Tech.*, vol. 37, pp. 1964–1972, Dec. 1989.

[7] D. M. Sheen, S. M. Ali, M. D. Abouzahra, and J. A. Kong, "Application of the three-dimensional finite-difference time-domain method to the analysis of planar circuits," *IEEE Trans. Microwave Theory Tech.*, vol. 38, pp. 849–857, July 1990.

[8] M. Maeda, "Analysis of gap in microstrip transmission lines," *IEEE Trans. Microwave Theory Tech.*, vol. MTT-20, pp. 390–396, June 1972.

[9] P. Benedek and P. Silvester, "Equivalent capacitance of microstrip gaps and steps," *IEEE Trans. Microwave Theory Tech.*, vol. MTT-20, pp. 729–733, Nov. 1972.

[10] P. Silvester and P. Benedek, "Equivalent capacitance of microstrip open circuits," *IEEE Trans. Microwave Theory Tech.*, vol. MTT-20, pp. 511–516, Aug. 1972.

[11] P. Silvester and P. Benedek, "Equivalent discontinuities capacitances for right-angle bends, t-junctions, and crossings," *IEEE Trans. Microwave Theory Tech.*, vol. MTT-21, pp. 341–346, May 1973.

[12] R. Horton, "The electrical characterization of a right-angle bends in microstrip line," *IEEE Trans. Microwave Theory Tech.*, vol. MTT-21, pp. 427–429, June 1973.

[13] T. Itoh, "Analysis of microstrip resonators," *IEEE Trans. Microwave Theory Tech.*, vol. MTT-22, pp. 946–952, Nov. 1974.

[14] I. Wolff, G. Kompa, and R. Mehran, "Calculation method for microstrip discontinuities and T-junctions," *Electron. Lett.*, vol. 8, 1972.

[15] G. Kompa and R. Mehran, "Planar waveguide model for calculating microstrip components," *Electron. Lett.*, vol. 11, 1975.

[16] W. Menzel and I. Wolff, "A method for calculating the frequency dependent properties of microstrip discontinuities," *IEEE Trans. Microwave Theory Tech.*, vol. MTT-25, pp. 107–112, Feb. 1977.

[17] A. Sommerfeld, *Partial Differential Equations in Physics*. New York: Academic Press, 1949.

[18] T. Itoh, *Numerical Techniques for Microwave and Millimeter-Wave Passive Structures*. New York: Wiley, 1989, pp. 137–140.

[19] M. Drissi, V. Fouad Hanna, and J. Citerne, "Theoretical and experimental investigation of open microstrip gap discontinuities," in *Proc. 18th European Microwave Conf.*, Sept. 1988, pp. 203–208.

[20] R. F. Harrington, *Field Computation by Moment Methods*. New York: Macmillan, 1968.

[21] A. C. Cangellaris, "The importance of skin-effect in microstrip lines at high frequencies," in *IEEE MTT-S Int. Microwave Symp. Dig.*, May 1988, pp. 197–198.

[22] T. E. van Deventer, P. B. Katehi, and A. C. Canggellaris, "An integral equation method for the evaluation of conductor and dielectric losses in high frequency interconnects," *IEEE Trans. Microwave Theory Tech.*, vol. 37, pp. 1964–1971, Dec. 1989.

[23] W. Wertgen and R. H. Jansen, "Novel Green's function database technique for efficient full-wave analysis of complex irregular (M)MIC-Structures," in *Proc. 19th European Microwave Conf.* Sept. 1989, pp. 199–204.

[24] W. Wertgen and R. H. Jansen, "Efficient direct and iterative electrodynamic analysis of geometrically complex irregular MIC and MMIC-structures," *Int. J. Numerical Modelling*, pp. 153–186, Sept. 1989.

[25] P. S. Hall and S. J. Vetterlein, "Microstrip patch array with multiple beams," in *Proc. 19th European Microwave Conf.*, Sept. 1989, pp. 343–348.

[26] R. E. Collin, *Foundations For Microwave Engineering*. New York: McGraw Hill, 1966, pp. 363–433.

[27] J. A. Weiss, "Dispersion and field analysis of a microstrip meander-line slow-wave structure," *IEEE Trans. Microwave Theory Tech.*, vol. MTT-22, pp. 1194–1201, Dec. 1974.

[28] V. Rizzoli and A. Lipparini, "Bloch-wave analysis of stripline- and microstrip-array slow-wave structures," *IEEE Trans. Microwave Theory Tech.*, vol. MTT-29, pp. 143–149, Feb. 1981.

[29] F. J. Glandorf and I. Wolff, "A spectral-domain analysis of periodically loaded non-uniform microstrip lines," *IEEE Trans. Microwave Theory Tech.*, vol. MTT-35, pp. 336–343, Mar. 1987.

[30] *Touchstone*, EESOF INC., Westlake Village, CA 91362.

✠

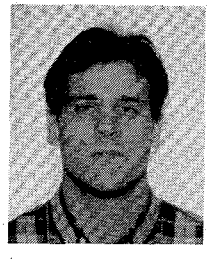

William P. Harokopus, Jr., (S'86–M'91) was born in Detroit, MI, on February 10, 1963. He received the B.S. (1985) and M.S. (1986) degrees in electrical engineering from the University of Michigan, Ann Arbor. He is currently pursuing the Ph.D. degree at Michigan, where he works in the Radiation Laboratory as a graduate research assistant. His dissertation will be on the high-frequency characterization of open microstrip discontinuities.

Linda P. B. Katehi (S'81–M'84–SM'89) received the B.S.E.E. degree from the National Technical University of Athens, Greece, in 1977 and the M.S.E.E. and Ph.D. degrees from the University of California, Los Angeles, in 1981 and 1984 respectively.

In September 1984 she joined the faculty of the Electrical Engineering and Computer Science Department of the University of Michigan, Ann Arbor. Since then, she has been involved in the modeling and computer-aided design of millimeter-wave and near-millimeter-wave monolithic circuits and antennas.

In 1984 Dr. Katehi received the W. P. King Award and in 1985 the S. A. Schelkunoff Award from the Antennas and Propagation Society. In 1987 she received an NSF Presidential Young Investigator Award and an URSI Young Scientist Fellowship. She is a member of Sigma Xi.